JOURNAL OF PROPULSION AND POWER
Vol. 18, No. 2, March–April 2002

Effect of Nozzle Cavity on Resonance in Large SRM: Theoretical Modeling

J. Anthoine* and J-M. Buchlin†
von Kármán Institute for Fluid Dynamics, 1640 Rhode-St-Genese, Belgium
and
A. Hirschberg‡
Technische Universiteit Eindhoven, 5600 MB Eindhoven, The Netherlands

Cold gas experiments are used to study the vortex–nozzle interaction, which drives thrust pulsation in solid-rocket motors. The experiments carried out in an axial flow model clearly demonstrate coupling of vortex shedding with acoustical longitudinal resonances of the combustion chamber as observed in actual motors. The amplitudes of the pressure fluctuations correspond to one-thousandth of the static pressure, which is the order of magnitude of the observed pulsations in rocket motors. Experiments show that the cavity formed around the nozzle inlet during combustion is crucial. The pulsation level is proportional to the volume of the cavity. Theory predicts this relationship if we assume vortex–nozzle interaction to be the main source of sound. The proposed analytical model does, however, overestimate the pulsation level by an order of magnitude.

Nomenclature

A = nozzle throat area
a = sound speed
D = internal diameter of the model
d = internal diameter of the inhibitor
f = frequency of the oscillation
He = Helmholtz number
h_c = width of the nozzle cavity entrance
L = total length
l = inhibitor–nozzle distance
M_0 = mean Mach number
$\dot{m}$ = mass flow rate per surface unit
$\mathcal{P}$ = average acoustic power
p_0 = mean static pressure
p' = oscillatory pressure
S = cross surface of the model
S_c = cross surface of the nozzle cavity entrance
Sr = Strouhal number
T = period of the oscillation
U_0 = mean flow velocity
u' = oscillatory velocity
V_c = nozzle cavity volume
$\boldsymbol{v}$ = vortex transport velocity vector
Z_n = impedance of the nozzle
Γ = vortex circulation
γ = ratio of specific heats
ρ_0 = mean density
$\boldsymbol{\omega}$ = vorticity vector

Subscripts

ac = acoustic
m = acoustic mode number

Received 30 April 2001; presented as Paper 2001-2102 at the AIAA/CEAS 7th Aeroacoustics Conference, Maastricht, The Netherlands, 28–30 May 2001; revision received 9 October 2001; accepted for publication 9 October 2001.

*Assistant Professor, Environmental and Applied Fluid Dynamics Department, Chaussée de Waterloo 72; anthoine@vki.ac.be. Member AIAA.
†Professor, Environmental and Applied Fluid Dynamics Department, Chaussée de Waterloo 72.
‡Professor, Physics Department, cc.2.24, N-Laag, Postbus 513.

Introduction

THE present research is an experimental and theoretical study of aeroacoustic phenomena occurring in large solid-rocket motors (SRM), such as the Ariane-5 boosters. The emphasis is on aeroacoustic instabilities that may lead to internal pressure and thrust oscillations that reduce the rocket motor performance and could damage the payload. The study is carried out within the framework of a Centre National d'Etudes Spatiales research program.

Large SRM have a submerged nozzle and segmented propellant grains separated by inhibitors (Fig. 1). During combustion, the regression of the solid propellant surrounding the nozzle integration leads to the formation of a cavity whose volume varies during the launch. The hot burnt gas flow in the combustion chamber originates radially from the burning surface and then develops longitudinally before reaching the exhaust nozzle. During combustion, the regression of the burning surface is faster than that of the inhibitor rings. Then, vortical flow structures may be formed from the inhibitor.[1] This type of hydrodynamic instability is called obstacle vortex shedding (OVS). In early studies of this type of oscillation, it was believed that the inhibitors were the only cause of the formation of vortices and of pulsations.[1,2]

Experiments with SRM with segmented propellant grains, in which these inhibitors had been removed, did show that pulsations could appear without the presence of inhibitors.[3] In such cases, it was the perturbation in the propellant surface between two grains that seem to trigger the formation of vortices. Actually, due to the gradient in stagnation pressure between the core of the flow (higher enthalpy) and the new gas emerging from the grain (lower enthalpy), there is a nonuniform velocity profile at a given section of the combustion chamber. In a first-order approximation, this velocity profile can be described by the flow as a semi-infinite tube with radial gas injection at a constant velocity on the side wall. This is called the Taylor flow.[4] It can be shown that such a flow is linearly unstable.[5] This has been confirmed by many researchers, who have provided more advanced theories.[6–8] The idea, therefore, emerged that such instabilities could occur even in the absence of segmentation, and this has been confirmed in both scaled experiments with hot gases[9] and recently in cold gas experiments where the combustion process is simulated by the injection of air through a porous wall.[1,10]

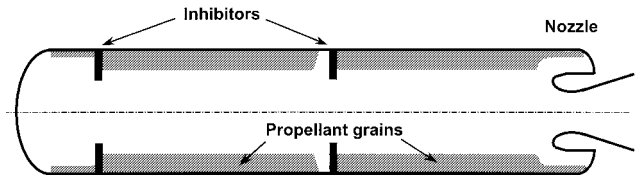

Fig. 1 Internal geometry of the Ariane-5 MPS of the actual combustion chamber.

The recent paper by Flandro[11] uses this concept of surface vortex shedding (SVS) to explain the instabilities in existing SRMs.

The hydrodynamic instabilities described (OVS and SVS) drive pressure oscillations in the combustion chamber of the motor. When the vortex shedding frequency is synchronized by acoustic modes of the motor chamber, resonant coupling may occur, leading to self-sustained oscillations. At full scale, pulsations correspond to an acoustical pressure amplitude of the order of $|p'|/p_0 = \mathcal{O}(10^{-3})$ of the static pressure $p_0 = \rho_0 a^2/\gamma$ in the reservoir. When an acoustical standing wave is assumed, this will correspond to acoustical velocity fluctuations (in plane waves), which are of the order of $|u'|/a \simeq |p'|/\gamma p_0 = \mathcal{O}(10^{-3})$ at the pressure nodes. For a main flow Mach number $U_0/a = \mathcal{O}(10^{-1})$, which is typical for the combustion chamber, this corresponds to $|u'|/U_0 = \mathcal{O}(10^{-2})$. Those acoustical velocity fluctuations induce viscous boundary layers with vorticity fluctuation, which are discussed in detail in the literature.[11]

These pressure oscillations have been reported for the Space Shuttle Redesigned Solid Rocket Motor, the Titan-34D SRM, the Titan-IV Solid Rocket Motor Upgrade, and the Ariane-5 Moteur à Propergol Solide.[1,3,12–14] All of these boosters have a length-over-diameter ratio (L/D) in the range 9–12 and demonstrated similar pressure oscillations, whatever the number of segments. Vortex-driven acoustically coupled oscillations were later observed on subscaled model rockets.[9,15,16] Numerical simulations have also brought further information on the aeroacoustic processes responsible for vortex-driven oscillations in SRMs.[17–20] These various studies point out that the frequency of oscillation increases as the grain surface rises. This observation typifies processes that depend on the velocity of the flow. The oscillations were, therefore, attributed to a periodic vortex shedding resulting from a strong coupling between the vortices and the acoustic field in the combustion chamber. It is suggested in the literature that vortex–nozzle interaction is the main aeroacoustical source in this feedback loop.[3]

The present research aims at investigating experimentally and theoretically the flow–acoustic coupling phenomena and, in particular, the effect of the nozzle cavity volume on the pressure pulsation level. Hence, we assume that the flow instabilities do occur and cannot be prevented, and we seek for a minimization of their impact. This is quite a different approach than a linear theory seeking for prediction of conditions at which oscillations do not occur at all. Our final aim is the understanding of the aeroacoustic phenomena that occur in the Ariane-5 booster.

Earlier Cold Gas Experiments

An early interpretation of the phenomenon is due to Flandro and Jacobs,[21] who linked the oscillations to the hydrodynamic instability of the sheared regions of the flow and to the coupled acoustical response of the motor. Because combustion is believed to take a minor part in the instability mechanism, most laboratory experiments were carried out with models operating with cold gases. Cold flow experiments in a pipe with one or two inhibitors were conducted, for example, by Culick and Magiawala,[22] Dunlap and Brown,[23] Hourigan et al.,[24] Mettenleiter et al.[25] and Anthoine.[26]

In these experiments, the vortex shedding is produced at the inhibitors, and the confined space of the pipe acts as a resonator with its natural frequencies. Pressure oscillation reaches large amplitude when the vortex shedding frequency is close to the frequency of one resonant acoustic mode of the system. Culick and Magiawala[22] showed that for their experiment it was impossible to sustain acoustic modes with only one inhibitor. The presence of an obstacle downstream of the shedding point of the vortices provides the necessary acoustical feedback when the vortices interact with it.[2,27] In the case of the Ariane-5 booster, this second obstacle could be the nozzle.

Another setup designed by Couton et al.[28] features a rectangular two-dimensional channel with wall injection, obstacles simulating inhibitor baffles, and a submerged nozzle. The channel resonance corresponding to the excitation of the first longitudinal modes and the amplification of the acoustic level was found to depend on the injected mass flow rate. Other experiments indicate that the process is also controlled by the relative positions of the vortex shedding region and the acoustic resonant mode structure. The acoustic mode triggers vortex shedding more effectively at locations where the acoustic pressure features a node and the acoustic velocity an antinode.[1,23] However, in the case of OVS vortex shedding from a sharp edge, a large acoustical velocity at the vortex shedding point leads to a large initial absorption that can reduce pulsation levels.[29] The optimal position for strong oscillation levels appears to be a compromise between initial absorption and strong feedback. It appears that, for rigid diaphragms, the vortex-generation point should be located close to an acoustic velocity antinode to optimize pulsations.

As discussed, the work of Vuillot et al.,[17] Dotson et al.,[3] and Casalis et al.[6] has indicated that the presence of inhibitors is not necessary to drive the oscillations. In our experiments, however, we will not have a radial cold gas injection, but rather an axial injection through the forward end of the model. In such a case, an inhibitor is placed to produce the necessary vortex shedding. We focus on the interaction of these vortices with the nozzle at the backward end of the model.

Flow–Acoustic Coupling

It is now well established that the flow–acoustic coupling observed in actual SRMs and in cold gas experiments can be described as a feedback loop consisting of five elements: 1) the hydrodynamic instability of vortical regions of the flow; 2) the roll-up, growth, and advection of vortices; 3) the generation of an acoustic perturbation due to the interaction of the vortices with an obstacle, such as the nozzle (acoustic source); 4) the acoustical response of the combustion chamber; and 5) the acoustical triggering of the shear flow instability.

The hydrodynamic instability of vortical regions of the flow leads to vortex formation (OVS and SVS). The coherence degree of these structures depends on the presence of an external acoustic field. When the vortices interact with a surface like the nozzle head, energy passes from the vortex to the acoustic field.[30] Part of this acoustical energy is fed back to the shear flow instability. The receptivity of the shear region to the acoustic modulations closes the loop, and a new vortex is shed. This receptivity is understood for OVS, but is the subject of research for SVS.

When the acoustical quality factor of the combustion chamber is low, the acoustical field is best described in terms of propagating waves. For high-quality factors, the sound field is best described in terms of standing acoustical waves (resonance mode). In the first case, wave propagation time from the sound source toward the vortex shedding point is essential in determining the phase condition for oscillation. This leads to oscillations at fixed Strouhal numbers $Sr_L = fL/u_0$ based on the flow velocity u_0 at the nozzle inlet. This could be called a noncompact edge tone type oscillation.[31] Such oscillations are observed in the initial phase of the combustion when the chamber diameter is close to the nozzle throat diameter, corresponding to high flow Mach numbers in the chamber. The oscillation modes are predicted by the well-known formula of Rossiter.[32]

As the combustion proceeds and the diameter of the chamber increases, a shift is observed toward typical resonant behavior. Oscillation frequencies f are close to the resonance frequencies. In first approximation, the acoustic standing wave can be modeled by that of a closed–closed pipe segment of length L. Hence, the resonances are expected close to Helmholtz numbers $He = fL/a = n/2, n = 1, 2, 3, \ldots$. The oscillation frequency will change slowly with the change in flow velocity. This change accounts for the necessary phase shift needed to compensate for the

change in travel time of vortical structures, which is needed to obtain a phase shift equal to an integer number of 2π along the feedback loop. This phenomena has been extensively described for deep cavities[33,34] and the flute.[35,36] We will, therefore, call this a flute behavior. In this particular case the term corresponding to the travel time of acoustic waves from the nozzle to the vortex shedding point should be removed from the formula of Rossiter.[32]

Limitation of Linear Theories

In a linear theory, the energy losses of the system by radiation, viscothermal effects, etc., are proportional to the square $(|p'|/p_0)^2$ of the pulsation amplitude. The aeroacoustical sound source produces an energy that is also proportional to the square $(|p'|/p_0)^2$ of the pulsation amplitude. Hence, we can distinguish three conditions predicted by linear theory: 1) stability, 2) neutrality, and 3) instability.

For a stable flow the losses are larger than the production, so that instabilities will be damped. For a neutral flow the losses are equal to the production, so that the amplitude of oscillation is fully determined by the initial conditions. There is neither growth nor damping. For unstable condition the losses are smaller than the production, so that the amplitude will increase exponentially with time. It is clear that in such a case the rocket should either explode or there should be another nonlinear saturation mechanism (than the destruction of the engine) in the feedback loop, which explains why a finite steady amplitude $|p'|/p_0$ is reached after some time.

Typically, due to confinement effects, the hydrodynamic wavelength of the vortical instability waves cannot be much larger than the diameter of the combustion chamber. This is confirmed by linear stability analysis.[6] According to the length-over-diameter ratio, there will be at least six hydrodynamic wavelengths between the point at which the hydrodynamic instabilities are triggered and the nozzle. The amplification of such hydrodynamic perturbations is huge. In the case of a free shear layer as produced at an inhibitor, the amplification is $e^{2\pi} = \mathcal{O}(5 \times 10^{-2})$ per wavelength. For instabilities of the Taylor profile, information is provided by Griffond et al.[7] It is clear that after six wavelengths even a very modest perturbation of order $|u'|/U_0 = \mathcal{O}(10^{-2})$, as will result from the observed acoustical oscillations (described earlier) will have become so large that a linear theory does not predict the unsteady flow at the nozzle.

Indeed, numerical simulations[17,20] do clearly show the breakdown within two hydrodynamic wavelengths of the flow into discrete vortices, a nonlinear saturation mechanism of the flow instability. Hence, whereas linear theory can be used to predict the condition at which oscillations might occur, once these oscillations do occur linear theory cannot describe the flow. Furthermore, in a self-sustained oscillation process, linear theory cannot predict a finite amplitude level of oscillations. Those are two arguments to consider in a nonlinear theory.

Discrete Vortex Models

Vortex–nozzle interaction can be studied numerically.[17,20,37] However, we seek a simple analytical model. In contrast to the work of Lovine and Waugh,[38] Vuillot,[17] Casalis et al.,[6] Griffond et al.,[7] Griffond and Casalis,[8] and Flandro and Majdalani,[11] we do not seek a prediction of conditions at which the combustion is stable. We assume that it is unstable, and we are looking for a way to minimize the thrust oscillations. A key point of our nonlinear approach is to assume that the structure of the vortices reaching the nozzle is independent of the acoustical amplitude. The vortex formation is triggered by the acoustical flow, but the vortices concentrate the vorticity of the entire flow. The acoustical perturbations have only a minor effect on the amount of vorticity and the path of the vortex at the nozzle.[39]

In the case of SRMs, Flandro[40] and Dotson et al.[3] suggest that sound is produced by the impingement of the vortices on the wall of the nozzle inlet. When vortices approach the nozzle inlet, their transport velocity vector is significantly deviated from the acoustical streamlines (potential flow). Following Howe,[41] they produce sound when this occurs. Hence, we should translate the impingement described by Flandro as vortex–sound interaction localized at the nozzle inlet.[42] We will now show that this interaction is stronger for a submerged nozzle because of the presence of the cavity.

We will make this plausible by means of an analytical model. The model is based on the vortex–sound theory developed by Powell[43] for subsonic flows in free-field conditions. Howe[44] proposed a generalization to internal flows. The vortex–sound theory assumes some existing knowledge of the vortical distribution in the flow and deduces the aeroacoustical sound production from this knowledge.[42] At low Mach numbers such as those occurring here, the time average acoustic power $\mathcal{P}$ is given by

$$\mathcal{P} = -\rho_0 \left\langle \int_V (\boldsymbol{\omega} \times \boldsymbol{v}) \cdot \boldsymbol{u}' \, \mathrm{d}V \right\rangle \tag{1}$$

where V is the source volume (where $\boldsymbol{\omega} \neq 0$). The brackets indicate the averaging over one period of a steady oscillation.

In Howe's approximation,[44] which is valid for a source that is small compared to the acoustic wavelength and at low Mach numbers, the vortices have the character of a dipole source. A dipole is associated with a force. In this case, the force density in the flow corresponds to the Magnus force on the fluid particles experienced by an observer moving with the fluid as a result of the Corriolis acceleration $-(\boldsymbol{\omega} \times \boldsymbol{v})$. The breakdown of the vorticity distribution into discrete vortices as described in the preceding paragraph implies that $(\boldsymbol{\omega} \times \boldsymbol{v})$ is independent of the amplitude $u' = |\boldsymbol{u}'|$ of the acoustical velocity. To perform acoustical work, this force needs an acoustical displacement of fluid particles. The power is proportional to the acoustical particle velocity $\boldsymbol{u}'$. If we assume that the acoustic field is represented by a resonant mode of a closed–closed pipe segment with a velocity node $(|u'| = 0)$ at the nozzle, we cannot understand that vortices produce any acoustical energy. It is actually the deviation of the actual acoustical flow from this crude model that does allow the vortices to produce acoustical energy. This is due to the presence of the cavity around the nozzle inlet for a submerged nozzle. Furthermore, the fact that the nozzle is not a closed wall will result into some acoustical energy losses by radiation, which we discuss later.

The vortex–sound theory yields the acoustic power given by Eq. (1) and representing the time average of the power transfer from the vorticity field to the acoustical field. When the vortex transport velocity vector $\boldsymbol{v}$ is parallel to the acoustic streamlines $(\boldsymbol{u}')$, the vectorial triple product in Eq. (1) vanishes. There is no acoustical energy production. To produce sound, the vortices should cross the acoustic streamlines, corresponding to the potential flow streamlines.[42] The larger is the angle between the two vectors, the stronger the acoustic production. We will further assume that the vortices follow a path as shown in Fig. 2. When the vortices travel in front of the cavity entrance, the acoustic velocity $\boldsymbol{u}'$ is almost normal to the vortex path $\boldsymbol{v}$. This vortex path will result in a maximum of sound production. Our model should, therefore, provide an upper bound for the pulsation amplitude. Furthermore, the acoustic power is stronger if the acoustic fluctuation u' is higher. The vortices should reach this point

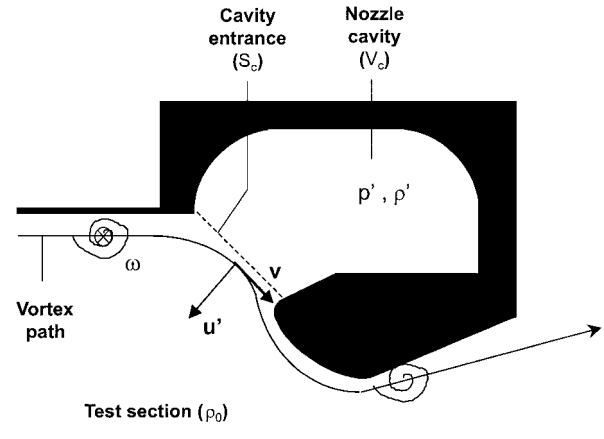

Fig. 2 Theoretical modeling of the vortex–nozzle interaction.

at the right time. As vortices are convected along the chamber, the acoustical field is directed in the direction of the vortex convection velocity and sound production will be weak. Sound production can occur as a result of vortex pairing, but this has a quadrupole character. We neglect such effects. Therefore, one should estimate the acoustic fluctuation u' induced by the nozzle cavity volume.

As will be shown in the experiment section, the nozzle cavity promotes higher resonance when the volume is larger. The compressibility of the gas in the cavity volume V_c induces an acoustic fluctuation u' in the cross section S_c (Fig. 2) such that, from mass conservation, it follows that

$$\rho_0 u' S_c \simeq \frac{V_c}{a^2}\frac{\mathrm{d}p'}{\mathrm{d}t} \tag{2}$$

where we made use of the cavity being small compared to the acoustical wave length ($\lambda \sim L$). The acoustic velocity u' is the component of $\boldsymbol{u}'$ normal to the vortex path taken positive when it is directed from the cavity toward the main flow.

Assuming a harmonically oscillating acoustic field ($u' = |u'|e^{i2\pi ft}$ and $p' = |p'|e^{i2\pi ft}$) and applying the perfect gas law ($\rho_0 a^2 = \gamma p_0$), one can write

$$|u'| = \frac{2\pi f V_c}{\gamma S_c}\frac{|p'|}{p_0} \tag{3}$$

The maximum of acoustic power is then expressed from Eq. (1) by

$$\mathcal{P}_{\max} \sim \rho_0 |\boldsymbol{v}||\boldsymbol{u}'| \int_V |\boldsymbol{\omega}|\,\mathrm{d}V \sim \rho_0 |\boldsymbol{v}||\boldsymbol{u}'|(\pi D\Gamma) \tag{4}$$

where Γ is the circulation of the vortex, $|\boldsymbol{v}|$ is approximated by half of the mean flow velocity $U_0/2$, and $|\boldsymbol{u}'|$ is given by Eq. (3). As explained earlier, in our model, vortices produce sound only when passing in front of the cavity entrance. We do expect that for maximum pulsation the vortex will pass along the cavity at the time corresponding to maximum power generation. A weighting coefficient has to be introduced in Eq. (4) to take into account the time fraction T_c during which the vortex travels in front of the cavity entrance compared to the vortex shedding period $T = 1/f$. This coefficient is equal to

$$\frac{T_c}{T} = \frac{2h_c/U_0}{1/f} = \frac{2h_c f}{U_0} \tag{5}$$

Then, when it is assumed that $T_c/T \ll 1$, the generated acoustical power becomes

$$\mathcal{P} \sim \rho_0 \frac{U_0}{2}\frac{2\pi f V_c}{\gamma S_c}\frac{|p'|}{p_0}\pi D\Gamma\frac{2h_c f}{U_0} \tag{6}$$

The cross section S_c of the cavity entrance can be assumed parallel to the test section axis, $S_c = \pi D h_c$ (Fig. 2). The circulation Γ is given by

$$\Gamma \sim l_v(U_0/2) \sim U_0^2/4f \tag{7}$$

where l_v is the distance in which the vortex accumulates vorticity, assumed to be equal to the distance between two successive vortices [$l_v \sim U_0/(2f)$]. When the perfect gas law $\rho_0 a^2 = \gamma p_0$ is assumed, Eq. (6) transforms to

$$\mathcal{P} \sim \rho_0 \frac{U_0}{2}\frac{2\pi f V_c}{\rho_0 a^2 \pi D h_c}|p'|\pi D\frac{U_0^2}{4f}\frac{2h_c f}{U_0} \tag{8}$$

or, after simplification,

$$\mathcal{P} \sim (\pi/2) M_0^2 f V_c |p'| \tag{9}$$

On the other hand, when it is assumed that the acoustic losses are dominated by the radiation at the nozzle, the acoustic power is the work of the fluctuating pressure per unit time, which can be expressed as

$$\mathcal{P} = \langle p'u' \rangle \frac{\pi D^2}{4} \sim \frac{|p'|^2}{2}\frac{\pi D^2}{4}\frac{1}{Z_n} \tag{10}$$

where

$$Z_n = (p'/u')_{\text{nozzle}} \tag{11}$$

This impedance is expected to be reasonably described by a quasi-stationary model.[45] The key idea is to calculate the fluctuations of the pressure at the nozzle inlet by means of a subsonic flow model and to consider the Mach number constant in spite of the pressure unsteadiness:

$$\mathrm{d}M_0 = 0 \rightarrow \mathrm{d}(u/a) = 0 \rightarrow (u'/u) = a'/a \tag{12}$$

Knowing that $a = \sqrt{(\gamma p/\rho)}$, and assuming isentropic evolution $p\rho^{-\gamma} = cst$, one gets

$$u'/u = a'/a = \tfrac{1}{2}(p/\rho)'/(p/\rho) = [(\gamma - 1)/2\gamma]p'/p \tag{13}$$

or, with $\gamma p = \rho a^2$,

$$\rho a u' = M_0[(\gamma - 1)/2]p' \tag{14}$$

Hence, the impedance of the nozzle reduces to

$$Z_n = \frac{2\rho a}{M_0(\gamma - 1)} \tag{15}$$

Therefore, when Eqs. (9), (10), and (15) are combined, the acoustic power is given by

$$\mathcal{P} \sim \frac{\pi}{2} M_0^2 f V_c |p'| \sim \frac{|p'|^2}{2}\frac{\pi D^2}{4}\frac{M_0(\gamma - 1)}{2\rho a} \tag{16}$$

leading to

$$|p'| \sim \frac{8\rho a}{(\gamma - 1)D^2} M_0 f V_c \tag{17}$$

or, by the use of the perfect gas law and equation $f/a = j/(2L)$,

$$|p'|/p_0 \sim [\pi\gamma/(\gamma - 1)]\, j M_0 (V_c/V_{\text{tot}}) \tag{18}$$

where

$$V_{\text{tot}} = (\pi D^2/4)L \tag{19}$$

When resonance occurs, the sound pressure level is a linear function of the Mach number, the excited mode number, and the nozzle cavity volume. In the next section we compare the results of this model with experimental data.

A weak point in our model is that we assume that the vortex trajectory remains independent of the geometry of the cavity. This appears to be reasonable in the present case. Note, furthermore, that if the acoustical energy losses are not dominated by the radiation at the nozzle, we will still find that $|p'| \sim V_c$, but not necessarily that $|p'| \sim M_0$.

Experimental Investigation

Experimental Setup

The experimental facility is a $\frac{1}{30}$-scale modular axisymmetric cold flow model of the Ariane-5 solid rocket motor, with a fully axial flow injected through the forward end. The model (in Fig. 3) consists of a cylindrical test section, with an inhibitor of orifice diameter d placed at a distance l from a nozzle with sonic condition at the throat.[26,46] The internal diameter D of the segments, equal to 0.076 m, is based on the $\frac{1}{30}$-scale similarity with the full-scale motor obtained by conserving the Mach number when 50% of the propellant is burnt. The total length L and the inhibitor parameters d and l can be modified. The test section is supplied with compressed air. The circulation of

the air along all of the connected pipes produces acoustic noise that could interact with the acoustic measurements carried out in the test section. The insertion of a porous plate at the forward end aims to ensure an acoustic insulation of the test section from the air supply, by providing a high-pressure drop.[46] This pressure drop is of the order of magnitude of the static pressure in the test section.

In the Ariane-5 booster, the flow–acoustic coupling is characterized by a shift of the instability mode frequency with respect to time and a frequency jump between the instability modes. Because the combustion is radial, the combustion chamber diameter increases with time, and the internal Mach number in the segments decreases. Therefore, flow–acoustic coupling is identified by plotting the evolution of the Strouhal number as a function of the Mach number, which is a measure of the combustion time.[3] A sonic throat nozzle ends the test section and the internal Mach number M_0 is defined, under low Mach number approximation, by

$$M_0 = \frac{U_0}{a} = \frac{\dot{m}}{\rho_f a} = \left[\frac{2+(\gamma-1)M_0^2}{\gamma+1}\right]^{(\gamma+1)/2(\gamma-1)} \frac{A}{S} = K\frac{A}{S} \tag{20}$$

where K depends only on the specific heat ratio (for cold air, $K = 0.58$). Thus, the only way to vary the Mach number M_0 is to modify the nozzle throat area A. We use a movable needle to control A (Fig. 3) (Ref. 46).

The flow–acoustic feedback loop relies on the interaction between the vortices and the nozzle. The nozzle geometry is then expected to play an important role in the amplification of the sound pressure fluctuations. Different nozzle geometries are designed. They are sketched in Fig. 4. Nozzle 1 is the submerged nozzle representing the actual nozzle geometry at $\frac{1}{30}$ scale. For the second nozzle, a part of the cavity is filled. The cavity volume is reduced by 49% and the cavity depth by 60%, changing slightly the total length of the test section. In the third nozzle, the cavity is filled up to the nozzle head. The nozzle lip has disappeared, but the backward facing step at the end of the segment is still present. The fourth nozzle has to be compared to the second one: The backward facing step disappeared after a segment of 76-mm diam was kept through the far end of the cavity. Comparing nozzles 3 and 4 to nozzle 2 will show whether the pressure fluctuations are more amplified by the presence of a nozzle lip or by the backward facing step. For nozzle 5, the lip geometry is changed compared to nozzle 2, whereas nozzle 6 is only the convergent-divergent section without a cavity. For all of these nozzles, the throat diameter is equal to 30 mm, and the convergent and divergent parts keep the same geometries. The only differences are coming from the cavity.

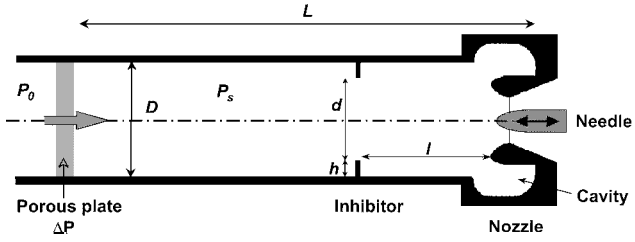

Fig. 3 Axisymmetric setup ($\frac{1}{30}$-scale).

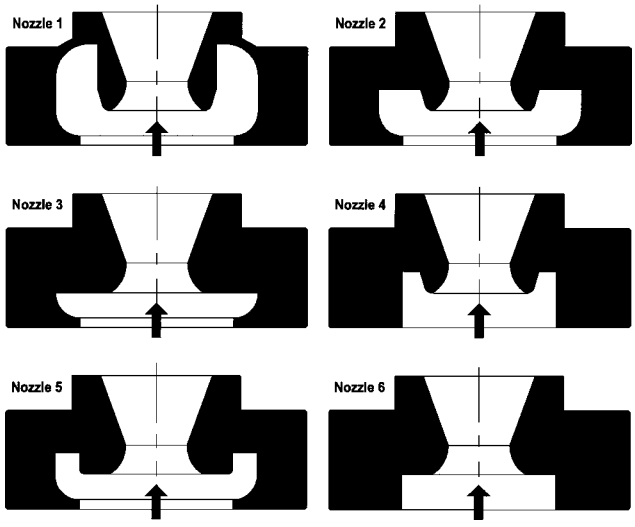

Fig. 4 Different exhaust nozzle geometries.

A piezoelectric pressure probe (PCB 106B60) from Piezotronics, Inc., allows measurement of the acoustic pressure fluctuations. The probe is placed just downstream of the porous plate. The acoustic pressure fluctuation data are acquired by means of a DAS1601 acquisition card controlled by Testpoint. The signals are filtered at 3 kHz and acquired at 7.5 kHz. 16,384 samples are saved on the disk and analyzed to determine the power spectrum of the pressure fluctuations. The spectrum is averaged on 7 blocks of 4096 data with an overlapping of 0.5. It gives a frequency resolution of 1.8 Hz.

Example of Flow–Acoustic Coupling

Figure 5a shows the pressure fluctuation spectrum plotted vs Mach number M_0 and frequency for an inhibitor of 58-mm internal diameter placed at 71 mm from the head of nozzle 1 with a cavity (Fig. 4). A peak is observed around 850 Hz and its frequency seems to vary linearly with the Mach number. This corresponds to a flute

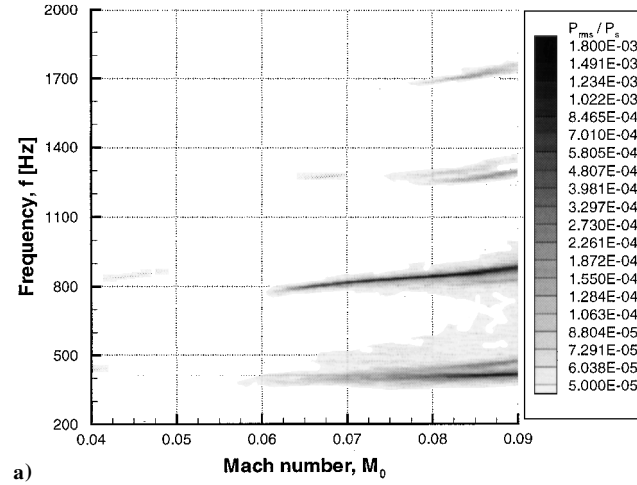

a)

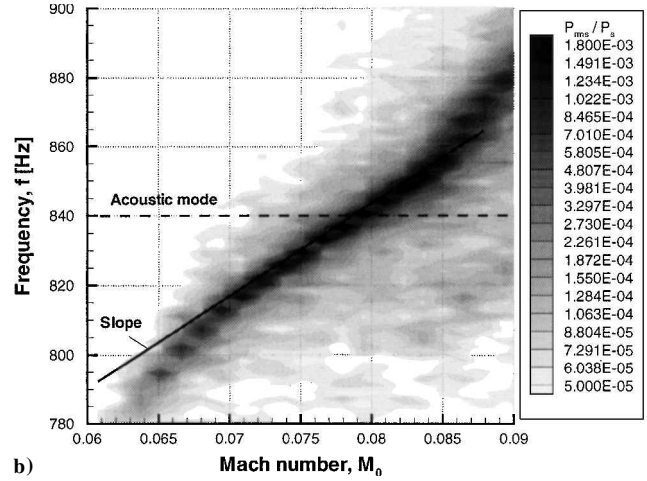

b)

Fig. 5 Distribution of the amplitude of a) pressure fluctuations and b) zoom between 780 and 900 Hz: L = 393 mm, l = 71 mm, and d = 58 mm, nozzle 1. The gray level indicates amplitude as shown by scale next to the graph.

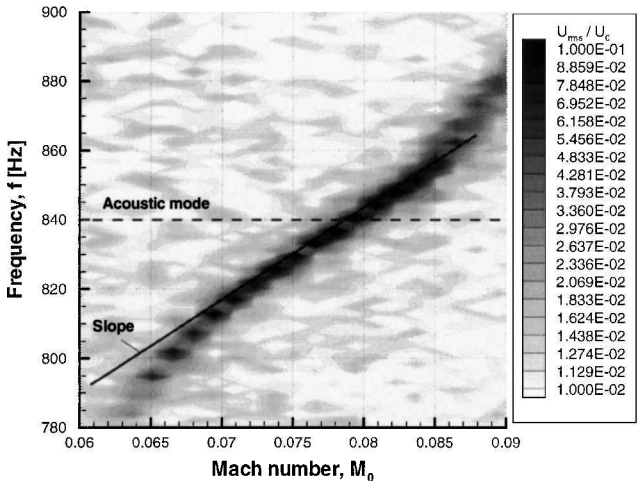

Fig. 6 Distribution of the amplitude of velocity fluctuations: L = 393 mm, l = 71 mm, and d = 58 mm, nozzle 1. The gray level indicates amplitude as shown by scale next to the graph.

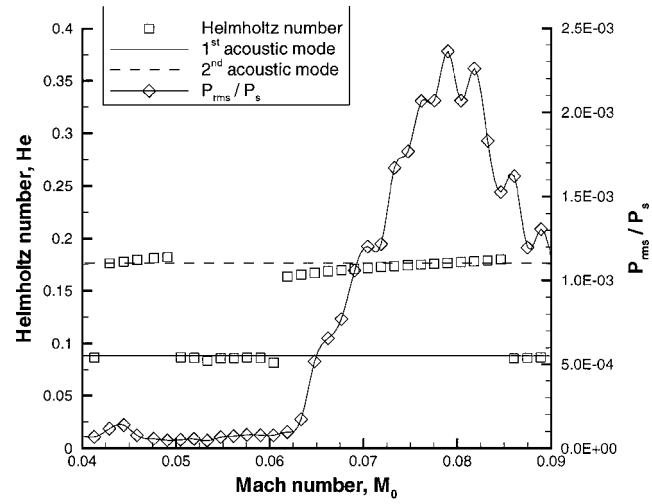

Fig. 7 Evolution of the maximum of the pressure fluctuation, in terms of Helmholtz number and amplitude: L = 393 mm, l = 71 mm, and d = 58 mm, nozzle 1.

mode as defined earlier. Creating a zoom between 780 and 900 Hz (Fig. 5b) shows that the slope of the evolution for Mach numbers between 0.072 and 0.082 is different than the slopes for lower or higher Mach numbers. In the Mach number range between 0.072 and 0.082, the frequency is very close to the second longitudinal acoustic mode frequency of the test section estimated by $f_{ac,2} = a/L$. The variation of the slope of the frequency evolution can only be produced by the acoustic resonance of the test section due to vortex shedding at that frequency. To confirm this affirmation, one has to demonstrate that the vortex shedding occurs at the second longitudinal acoustic mode frequency.

Figure 6 shows the contour of the velocity fluctuations measured with the hot wire located at 13 mm from the wall and at 37.5 mm downstream the inhibitor. There, the hot wire is on the path of the vortices shed by the inhibitor. The velocity fluctuations induced by the acoustic waves are negligible compared to those generated by the flow [$|u'|/U_0 = \mathcal{O}(10^{-2})$] (Ref. 47). The hot-wire signal is mainly determined by the vortical velocity fluctuations produced by the flow and not by the acoustics. Therefore, the spectrum of the signal acquired with the hot wire (Fig. 6) allows determination of the vortex shedding frequency. That frequency appears to correspond to the second longitudinal acoustic mode frequency (Fig. 5b). Thus, vortex shedding occurs at one of the acoustic mode frequency and excites the acoustic properties of the test section. Furthermore, the resonance modifies the vortex shedding frequency evolution (Fig. 6). Without acoustic resonance, the slope of the vortex shedding frequency evolution would correspond to a constant Strouhal number. This is observed by Dotson et al.[3] during the initial phase of the combustion. These observations prove the occurrence of a flow–acoustic coupling of the flute type in our model.

Figure 5a can also be plotted in term of Helmholtz number $He = fl/a$ instead of frequency f. Because l and a are constant, He is a nondimensional representation of the pressure fluctuation frequency. The maximums of the pressure fluctuation values are plotted vs Mach number in Fig. 7. The evolution of the Helmholtz number corresponding to the maximum of the pressure fluctuations is also given in Fig. 7. In such a plot, the longitudinal acoustic modes of the test section characterized by $He_{ac,j} = jl/(2L)$ correspond to horizontal lines. For such test conditions, each time the excited frequency is close to an acoustic mode frequency, the pressure fluctuation level is large. The maximum is reached when it crosses the acoustic mode.

When Fig. 7 is considered, the maximum of the sound pressure level is observed experimentally to excite the second mode at a Mach number M_0 equal to 0.08. It is worth applying an analytical model developed deliberately and based on Rossiter's approach[32] to compare the M_0 value at which the maximum of the sound pressure level is observed. That model[26] provides a relation linking the Mach number M_0, at which flow–acoustic coupling is predicted to occur, to the excited mode number j, the stage number m, the relative position of the inhibitor compared to the total length of the chamber l/L, and the relative internal diameter of the inhibitor compared to the chamber diameter d/D,

$$M_0 = C_{\mathrm{vc}}/2k_v[j/(m - 0.25)](l/L)(d/D)^2 \qquad (21)$$

where C_{vc} is the vena contracta coefficient of the jet generated by the inhibitor, and k_v is the ratio of the vortex transport velocity to the jet velocity. From the experimental investigation of the vortex properties in axial flow conditions reported in Ref. 39, it turns out that $C_{\mathrm{vc}} = 0.68$ and $k_v = 0.47$. From Eq. (21), a flow–acoustic coupling is predicted to occur at a Mach number equal to 0.086 on the second acoustic mode with two vortices located between the inhibitor and the nozzle. Such a finding is in good agreement with numerical simulations[20] and experimental observation obtained from particle image velocimetry measurements.[39]

Nozzle Design Effect

The flow–acoustic feedback identified in the preceding paragraph relies on the interaction between the vortices and the nozzle. Therefore, the nozzle geometry is expected to play an important role in the establishment of the amplitude of the sound pressure fluctuations. Indeed, by changing the nozzle design, the downstream obstacle at which vortices generate acoustic waves is modified.

The main characteristic of the nozzle used in the preceding section appeared to be the presence of a cavity around the convergent part of the nozzle, as depicted in Fig. 1. The present section is devoted to analyzing the effect of the nozzle cavity on the sound pressure levels. In the first part, different nozzle geometries are compared in terms of pressure fluctuations measured at the forward end of the test section. When the cavity volume is large enough, the longitudinal acoustic modes of the test section are not the only modes to be excited. Another frequency corresponding to the excitation of a localized acoustical mode of the nozzle cavity is also observed. That phenomenon is not discussed further because it does not correspond to pulsations observed in the actual rocket motor.

Pressure fluctuations are measured for an inhibitor with orifice diameter of $d = 0.058$ m placed at a distance $l = 0.071$ m from the head of the nozzle. The exact value of the length L of the test section depends on the nozzle geometry and is around $L = 0.38$ m. The maximum pressure fluctuation amplitudes are plotted vs Mach number M_0 in Fig. 8a for all of the nozzles with a throat diameter of 30 mm. The evolution of the Helmholtz number ($He = fl/a$) corresponding to the maximum of the pressure fluctuations is given in Fig. 8b where the horizontal lines correspond to the theoretical acoustic modes of the test section.

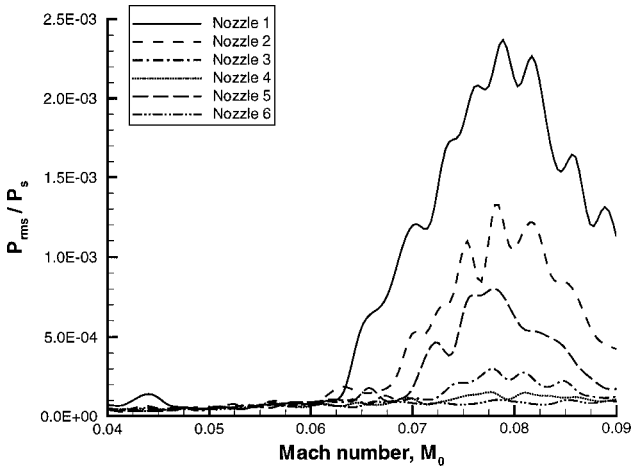

a) Pressure fluctuation level

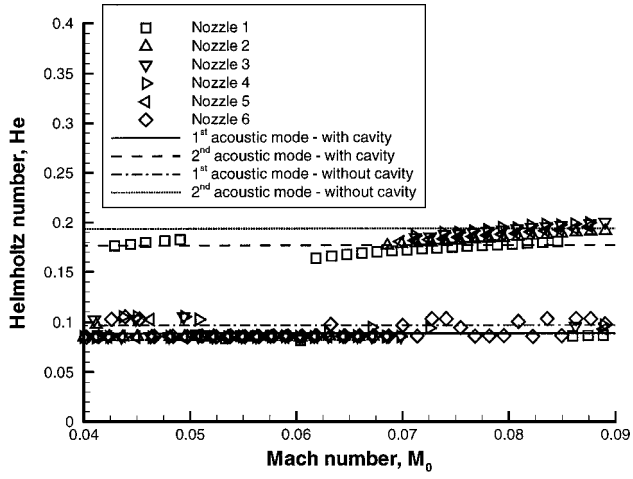

b) Helmholtz number

Fig. 8 Evolution of the maximum pressure fluctuations for nozzles 1–6: l = 0.071 m and d = 0.058 m.

The evolution of the Helmholtz number is similar for all of the nozzles except for nozzle 6, without a cavity. That means that the vortex shedding does excite the second longitudinal acoustic mode within the same Mach number range for all of the nozzles. The maximum sound pressure levels that correspond to the maximum of coupling appear at $M_0 = 0.08$, whatever the nozzle geometry. However, the amplitude of the maximum resonance depends on the nozzle design.

The maximum pressure fluctuation is plotted vs Mach number for the different nozzle geometries in Fig. 8b. The order of magnitude of the pulsation levels correspond to the data on pressure fluctuations in SRM reported in the literature.[3] When the nozzle cavity volume decreases (from nozzle 1 to 2), the pressure fluctuation drops. Filling the cavity up to the nozzle head (nozzle 3) has the effect of reducing the pressure level by a factor of 5 compared to nozzle 2. Nozzle 4 is obtained from nozzle 2 by removing the backward facing step at the end of the segment. Under such conditions, the pressure level is reduced by a factor of 10 and the amplitude measured for nozzle 4 is similar to that obtained for the nozzle without a cavity (nozzle 6). Without a cavity, the pressure fluctuation levels remain similar whatever the Mach number, indicating that vortex–acoustical coupling has disappeared. Finally, the effect of the nozzle head geometry is shown by nozzle 5. This nozzle presents a smaller cavity volume than nozzle 2, which results in fainter pressure fluctuations compared to nozzle 2.

The cavity volume plays an important role in the pressure fluctuations' magnitude as expected from the application of the vortex–sound theory discussed earlier. That effect is summarized in Fig. 9. Only the nozzles presenting a cavity and excitation on the second

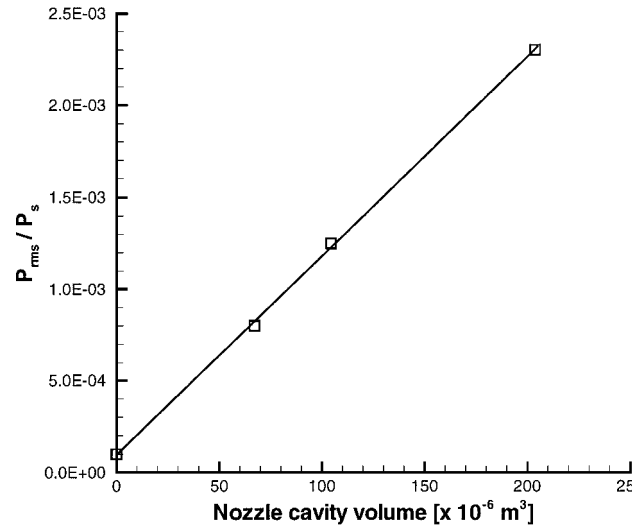

Fig. 9 Evolution of the maximum sound pressure level vs the nozzle cavity volume for excitation on the second acoustic mode at M_0 = 0.08: l = 71 mm and d = 58 mm.

acoustic mode at $M_0 = 0.08$ are considered. The evolution of the maximum sound pressure level is approximately linear with the nozzle cavity volume. Such a finding is in agreement with relation (18). The amplitude predicted by our model, however, is too large by two orders of magnitude. The measurements did not allow verification of the predicted Mach number dependence. This could be due to the existence of acoustical energy losses in the cavity, which are more important than the radiation losses at the nozzle. The trajectory of the vortex at the nozzle inlet is, furthermore, strongly influenced by the upstream configuration,[20] which should be taken into account for a quantitative prediction of amplitude.

Conclusions

Experimental data obtained in a cold gas model of a solid-propellant rocket motor has been presented. The data clearly demonstrate the occurrence of a flute mode in which vortex shedding at a diaphragm couples with acoustical resonances of the cavity. The order of magnitude of the amplitude of the pulsation corresponds to those observed in actual motors and depends strongly on the design of the nozzle. In particular, when an integrated nozzle is used, the pulsation increases linearly with the volume of the cavity formed around the nozzle inlet. This linear dependence is explained by a simple analytical model based on vortex sound theory. The amplitude, however, cannot yet be predicted by our model. These experiments also indicate that sound is not necessarily produced by an actual impingement of the vortices with the nozzle, but is rather a continuous process during the approach of the vortex. The sound produced during vortex ingestion by the nozzle might be less important.

Acknowledgments

This study has been supported by ESA and Centre National d'Etudes Spatiales (CNES). It is a part of a research program coordinated by CNES and ONERA.

References

[1]Brown, R. S., Dunlap, R., Young, S. W., and Waugh, R. C., "Vortex Shedding as a Source of Acoustic Energy in Segmented Solid Rockets," *Journal of Spacecraft*, Vol. 18, No. 4, 1981, pp. 312–319.

[2]Flatau, A., and VanMoorhem, W., "Prediction of Vortex Shedding Responses in Segmented Solid-Rocket Motors," AIAA Paper 90-2073, 1990.

[3]Dotson, K. W., Koshigoe, S., and Pace, K. K., "Vortex Shedding in a Large Solid-Rocket Motor Without Inhibitors at the Segmented Interfaces," *Journal of Propulsion and Power*, Vol. 13, No. 2, 1997, pp. 197–206.

[4]Taylor, G. I., "Fluid Flow in Regions Bounded by Porous Surfaces," *Proceedings of the Royal Society of London, Series A: Mathematical and Physical Sciences*, Vol. 234, No. 1199, 1956, pp. 456–475.

[5]Varapaev, V. N., and Yagodkin, V. I., "Flow Stability in a Channel with Porous Walls," *Izvestiya Akademii Nauk SSSR, Meckanika Zhidkostii Gaza [Fluid Dynamics]*, Vol. 4, No. 5, 1969, pp. 91–95.

[6]Casalis, G., Avalon, G., and Pineau, J.-Ph., "Spatial Instability of Planar Channel Flow with Fluid Injection Through Porous Walls," *Physics of Fluids*, Vol. 10, No. 10, 1998, p. 2558.

[7]Griffond, J., Casalis, G., and Pineau, J.-Ph., "Spatial Instability of Flow in a Semiinfinite Cylinder with Fluid Injection Through Its Porous Walls," *European Journal of Mechanics B—Fluids*, Vol. 19, No. 1, 2000, pp. 69–87.

[8]Griffond, J., and Casalis, G., "On the Nonparallel Stability of the Injection Induced Two-Dimensional Taylor Flow," *Physics of Fluids*, Vol. 13, No. 6, 2001, pp. 1635–1644.

[9]Prévost, M., Vuillot, F., and Traineau, J. C., "Vortex Shedding Driven Oscillations in a Subscale Motor for the Ariane 5 MPS Solid-Rocket Motors," AIAA Paper 96-3247, July 1996.

[10]Anthoine, J., Yildiz, D., and Buchlin, J.-M., "Nozzle Geometry Effect on the Instabilities in a Radial Injected Cold Flow Model of Solid-Propellant Boosters," *Proceedings of the 2nd European Symposium on Launcher Technology, Space Solid Propulsion*, Nov. 2000.

[11]Flandro, G. A., and Majdalini, J., "Aeroacoustic Instability in Rockets," AIAA Paper 2001-3868, July 2001.

[12]Mason, D. R., Folkman, S. L., and Behring, M., "Thrust Oscillations of the Space Shuttle Solid-Rocket Booster Motor During Static Tests," AIAA Paper 79-1138, June 1979.

[13]Blomshield, F. S., and Mathes, H. B., "Pressure Oscillations in Post–Challenger Space Shuttle Redesigned Solid-Rocket Motors," *Journal of Propulsion and Power*, Vol. 9, No. 2, 1993, pp. 217–221.

[14]Scippa, S., Pascal, P., and Zanier, F., "Ariane–5 MPS: Chamber Pressure Oscillations Full-Scale Firings Results Analysis and Further Studies," AIAA Paper 94-3068, June 1994.

[15]Vuillot, F., Traineau, J. C., Prévost, M., and Lupoglazoff, N., "Experimental Validation of Stability Assessment Methods for Segmented Solid-Propellant Motors," AIAA Paper 93-1883, June 1993.

[16]Traineau, J. C., Prévost, M., Vuillot, F., Le Breton, P., Cuny, J., Preioni, N., and Bec, R., "Subscale Test Program to Assess the Vortex Shedding Driven Instabilities in Segmented Solid-Rocket Motors," AIAA Paper 97-3247, July 1997.

[17]Vuillot, F., "Votex-Shedding Phenomena in Solid-Rocket Motors," *Journal of Propulsion and Power*, Vol. 11, No. 4, 1995, pp. 626–639.

[18]Kourta, A., "Shear Layer Instability and Acoustic Interaction in Solid-Propellant Rocket Motors," *International Journal for Numerical Methods in Fluids*, Vol. 25, No. 8, 1997, pp. 973–981.

[19]Mombelli, C., Guichard, A., Godfroy, F., and Guéry, J.-F., "Parallel Computation of Vortex Shedding in Solid-Rocket Motors," AIAA Paper 99-2510, June 1999.

[20]Anthoine, J., Buchlin, J.-M., and Guéry, J.-F., "Experimental and Numerical Investigations of Nozzle Geometry Effect on the Instabilities in Solid-Propellant Boosters," AIAA Paper 2000-3560, July 2000.

[21]Flandro, G. A., and Jacobs, H. R., "Vortex-Generated Sound in Cavities," AIAA Paper 73-1014, Oct. 1973.

[22]Culick, F. E. C., and Magiawala, K., "Excitation of Acoustic Modes in a Chamber by Vortex Shedding," *Journal of Sound and Vibration*, Vol. 64, No. 3, 1979, pp. 455–457.

[23]Dunlap, R., and Brown, R. S., "Exploratory Experiments on Acoustic Oscillation Driven by Periodic Vortex Shedding," *AIAA Journal*, Vol. 19, No. 3, 1981, pp. 408, 409.

[24]Hourigan, K., Welsh, M. C., Thompson, M. C., and Stokes, A. N., "Aerodynamic Sources of Acoustic Resonance in a Duct with Baffles," *Journal of Fluids and Structures*, Vol. 4, No. 4, 1990, pp. 345–370.

[25]Mettenleiter, M., Haile, E., and Candel, S., "Adaptive Control of Aeroacoustic Instabilities," *Journal of Sound and Vibrations*, Vol. 230, 2000, pp. 761–781.

[26]Anthoine, J., "Experimental and Numerical Study of Aeroacoustic Phenomena in Large Solid-Propellant Boosters," Ph.D. Dissertation, Free Univ. of Brussels, Brussels, Belgium, Oct. 2000.

[27]Schachenmann, A., and Rockwell, D., "Self-Sustained Oscillations of Turbulent Pipe Flow Terminated by an Axisymmetric Cavity," *Journal of Sound and Vibrations*, Vol. 73, No. 1, 1980, pp. 61–72.

[28]Couton, D., Plourde, F., and Doan, S., "Analysis of Energy Transfers of a Sheared Flow Generated by Wall Injection," *Experiments in Fluids*, Vol. 26, No. 3, 1999, pp. 222–232.

[29]Hirschberg, A., Bruggeman, J. C., Wijnands, A. P. J., and Smits, N., "The Whistler Nozzle and Horn as Aero-Acoustic Sound Sources in Pipe Systems," *Acustica*, Vol. 68, No. 2, 1989, pp. 157–160.

[30]Howe, M. S., *Acoustics of Fluid–Structure Interactions*, Cambridge Univ. Press, Cambridge, England, U.K., 1998.

[31]Powell, A., "On the Edge Tone," *Journal of Acoustical Society of America*, Vol. 33, 1961, pp. 395–409.

[32]Rossiter, J. E., "Wind Tunnel Experiments on the Flow over Rectangular Cavities at Subsonic and Transonic Speeds," Aeronautical Research Council, Ministry of Aviation, Repts. and Memoranda 3438, London, 1964.

[33]Rockwell, D., and Naudascher, E., "Self-Sustained Oscillations of Flow Past Cavities," *Journal of Fluids Engineering*, Vol. 100, No. 2, 1978, pp. 152–165.

[34]Bruggeman, J. C., Hirschberg, A., van Dongen, M. E. H., and Wijnands, A. P. J., "Self-Sustained Aero-Acoustic Pulsations in Gas Transport Systems: Experimental Study of the Influence of Closed Side Branches," *Journal of Sound and Vibrations*, Vol. 150, No. 3, 1991, pp. 371–393.

[35]Flechter, N. H., and Rossing, T., *The Physics of Musical Instruments*, 2nd ed., Springer–Verlag, New York, 1998.

[36]Verge, M. P., Causé, R., Fabre, B., Hirschberg, A., Wijnands, A. P. J., and Steenbergen, A., "Jet Oscillations and Jet Drive in Recorder-Like Instruments," *Acta Acustica*, Vol. 2, No. 5, 1994, pp. 403–419.

[37]Hulshoff, S. J., Hirschberg, A., and Hofmans, G. C. J., "Sound Production of Vortex Nozzle Interaction," *Journal of Fluid Mechanics*, Vol. 439, 2001, pp. 335–352.

[38]Lovine, R. L., and Waugh, R. C., "Standard Stability Prediction Method for Solid-Rocket Motors," Chemical Propulsion Information Agency, Johns Hopkins Univ., Columbia (MD) Publ. 273, 1975.

[39]Anthoine, J., Mettenleiter, M., Repellin, O., Buchlin, J.-M., and Candel, S., "Influence of Adaptive Control on Vortex Driven Instabilities in a Scaled Model of Solid Propellant Motors," *Journal of Sound and Vibration* (to be published).

[40]Flandro, G. A., "Vortex Driving Mechanism in Oscillatory Rocket Flows," *Journal of Propulsion and Power*, Vol. 2, No. 3, 1986, pp. 206–214.

[41]Howe, M. S., "The Dissipation of Sound at an Edge," *Journal of Sound and Vibration*, Vol. 70, No. 3, 1980, pp. 407–411.

[42]Hirschberg, A., Hulshoff, S., van Hassel, R. R., and Anthoine, J., "Vortex-Acoustic Interaction in Internal Flows: The Whistler-Nozzle, Human Whistling and the Solid-Propellant Rocket Motor," *Proceedings of the 3ème Colloque R&T CNES/ONERA* "*Ecoulements Internes en Propulsion Solide*," Ecole Nationale Supérieure de Mécanique et d'Aérotechnique, Vol. 3, 1998, p. 1.

[43]Powell, A., "Theory of Vortex Sound," *Journal of Acoustical Society of America*, Vol. 36, No. 1, 1964, pp. 177–195.

[44]Howe, M. S., "Contributions to the Theory of Aerodynamic Sound, with Application to Excess Jet Noise and the Theory of the Flute," *Journal of Fluid Mechanics*, Vol. 71, 1975, pp. 625–673.

[45]Vuillot, F., Tissier, P. Y., and De Amicis, R., "Stability Prediction for Large Segmented Solid Propellant Rocket Motors," *Proceedings of the AAAF, 5ème Symposium International sur la Propulsion dans les Transports Spatiaux*, ONERA TP 1996-045, 1996.

[46]Anthoine, J., and Olivari, D., "Cold Flow Simulation of Vortex Induced Oscillations in a Model of Solid-Propellant Boosters," AIAA Paper 99-1826, May 1999.

[47]Mettenleiter, M., "Contrôle Adaptatif des Propulseurs Segmentés," Ph.D. Dissertation, Ecole Centrale Paris, Paris, Feb. 2000.